

Optically detected and radio wave-controlled spin chemistry in cryptochrome

Kun Meng^{1,2}, Linyan Nie^{1,2†}, Johannes Berger^{3†}, Nick R. von Grafenstein^{1,2}, Christopher Einholz³, Roberto Rizzato^{1,2}, Erik Schleicher³, Dominik B. Bucher^{1,2*}

¹ Technical University of Munich, TUM School of Natural Sciences, Chemistry Department, Lichtenbergstr. 4, 85748 Garching bei München, Germany

² Munich Center for Quantum Science and Technology (MCQST), Schellingstr. 4, 80799, München, Germany

³ Institute of Physical Chemistry, Albert Ludwigs-Universität Freiburg, 79104 Freiburg, Germany

†These authors contributed equally to this work

*Corresponding author: dominik.bucher@tum.de

Abstract

Optically addressable spin systems, such as nitrogen-vacancy centers in diamond, have been widely studied for quantum sensing applications. In this work, we demonstrate that flavin-based cryptochrome proteins, which generate radical pairs upon optical excitation, also exhibit optically detected magnetic resonance. We further show that this optical spin interface is tunable by the protein structure. These findings establish radical pairs in proteins as a novel platform for optically addressable spin systems and magnetic field sensors. Additionally, the ability to control spin transitions introduces a new class of biophysical tools that hold promise for enabling multiplexed fluorescence microscopy. Importantly, due to the spin-selective nature of radical pair chemistry, the results lay the groundwork for radiofrequency-based manipulation of biological systems.

Main Text

Solid-state spins in semiconductors, such as the nitrogen-vacancy (NV) center in diamond¹ or boron vacancy in hexagonal boron nitride² are the workhorses of quantum sensing³ (Fig. 1a). Their spin-photon interface enables optically detected magnetic resonance (ODMR) for various sensing applications in biology and physics. Despite their great properties, synthetic tunability of their optical and spin properties or deterministic fabrication methods have remained elusive⁴. In contrast, molecular spin systems offer a compelling alternative, allowing bottom-up design with two key advantages: i) tunability through precise atomistic control over the molecular structure and its associated properties, and ii) scalability through chemical assembly. Recently, the synthesis of organometallic molecules with an optical spin interface has been demonstrated⁵. In our work, we show that certain proteins, specifically, cryptochrome, also exhibit optically addressable spin states. The main advantage of the genetically encoded protein scaffolds is their biocompatibility and their tunability via rational design⁶ or directed evolution⁷.

Photoactive flavin-containing proteins, such as photolyases and cryptochromes, are known to respond to blue light by forming spin-correlated radical pairs (RPs)⁸ (Fig. 1b). In photolyases, these RPs enable DNA repair⁹, while in cryptochromes they are thought to aid in magnetoreception, allowing birds to navigate along Earth's magnetic field^{8,10,11}. In the latter proteins, the RP consists of the flavin adenine dinucleotide (FAD) and a tryptophan (Trp) radical located on the surface of the protein, separated by ~ 2.1 nm¹².

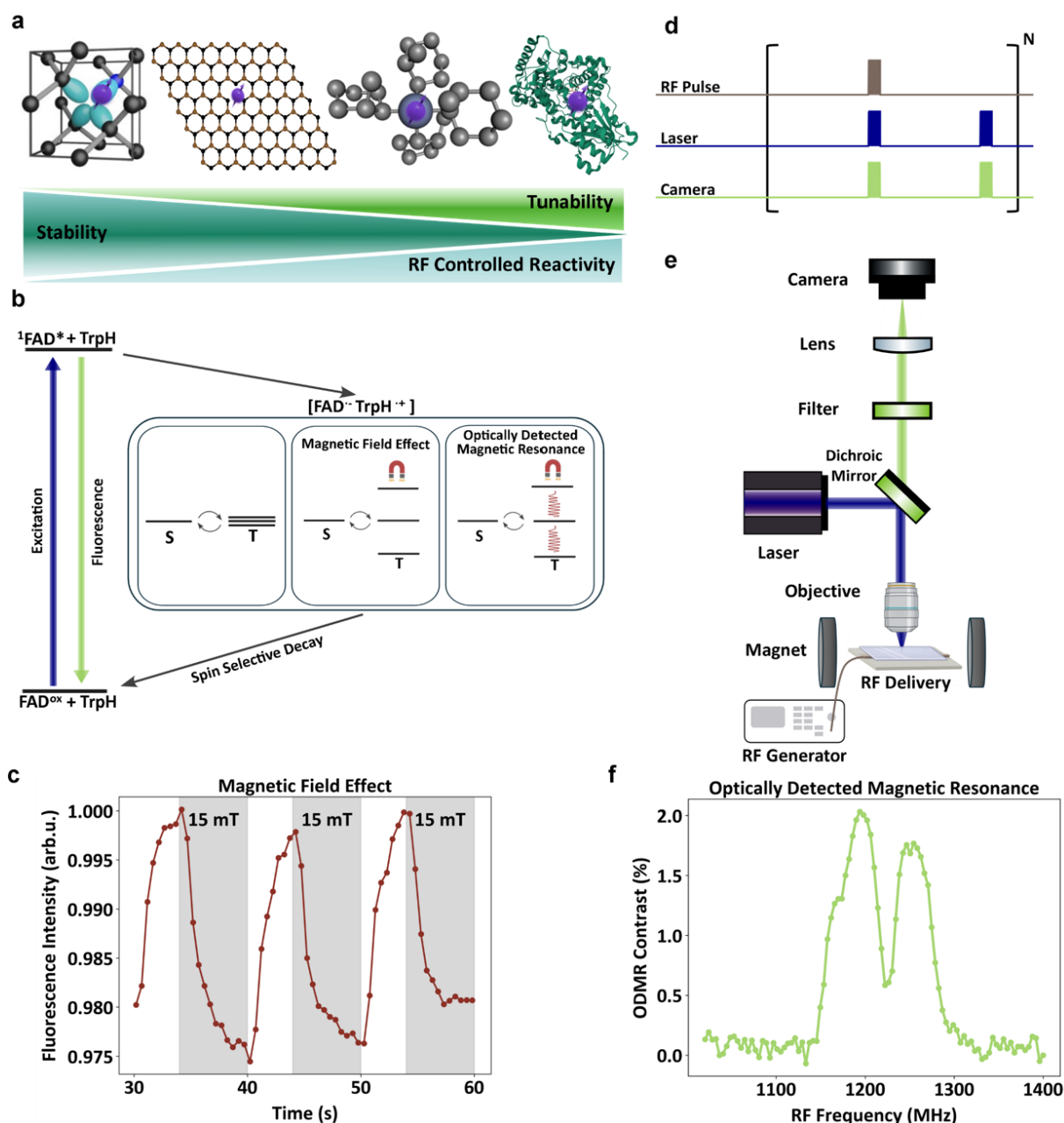


Figure 1. Optically addressable spin systems. **a)** Overview of various spin systems, including the nitrogen-vacancy center in diamond, the boron vacancy in hexagonal boron nitride, organo-metallic molecules, and, as demonstrated in this work, proteins. The degree of tunability increases from semiconductor-based systems to biological systems. Radical pairs and their yields in chemical and biological systems can be controlled by radio wave fields. **b)** Simplified schematic of the photophysical and spin dynamics of a photoinduced spin-correlated radical pair (RP). The interconversion between triplet and singlet states can be influenced by magnetic fields (magnetic field effect, MFE) or radio frequencies (optically detected magnetic resonance, ODMR), which impacts spin selective decay channels. **c)** Magnetic field effect observed in *Drosophila melanogaster* cryptochrome (*DmCry*). **d)** ODMR pulse sequence. **e)** Experimental setup of the ODMR experiments. **f)** ODMR spectrum of *DmCry*.

In a first step, we measured the FAD fluorescence of *Drosophila melanogaster* cryptochrome (*DmCry*) as a function of the applied magnetic field strength (Fig. 1c). We observed that the

fluorescence intensity is affected by the magnetic field, a phenomenon known as magnetic field effect, which can be described by the modulation of the singlet-triplet interconversion of the formed RP^{10,13} (Fig. 1b). Details and reference experiments can be found in Supplementary Note 1.

While this effect has been studied in detail previously, it inspired us to perform ODMR experiments, similar to their optically active solid-state spin counterparts. In these experiments, radio or microwave (RF) frequencies are used to address spin transitions that couple to the optical transitions and can be read out from the fluorescence intensity. Therefore, we have constructed a modified ODMR setup¹⁴ that includes temperature-controlled sample handling, a tunable magnetic field B_0 , and electronics for RF delivery, combined with sensitive fluorescence detection (see Materials and Methods) (Fig. 1e). In these experiments, fluorescence intensity is detected as a function of RF frequency. A typical ODMR pulse sequence is shown in Figure 1d, where we apply a specific RF frequency and simultaneously record the fluorescence intensity. To cancel noise (e.g., laser intensity fluctuations), a reference measurement is recorded without the RF pulse. We apply a magnetic field of approximately 43.2 mT, sweep the RF frequency from 1000 to 1400 MHz, and monitor the fluorescence intensity of the *DmCry* sample. An enhanced fluorescence intensity is observed around 1210 MHz, corresponding to the expected spin transition of a free electron (Fig. 1f). The experimental conditions have been optimized for the maximum contrast (details in Supplementary Note 2). Interestingly, we detect at least two peaks separated by ~ 50 MHz. This splitting is larger than the dipolar coupling strength between the two radicals reported in the literature (~ 8 MHz)¹². Therefore, the features observed in the spectrum are more likely due to a complex hyperfine network, which involves various nuclear spins within both the FAD and Trp radicals¹⁵.

To verify that the origin of the signal is caused by electron spin resonance, we calibrated the experiment and the magnetic field strength B_0 . We use a previously characterized solid-state spin system ($S=1/2$) in boron nitride nanotubes (BNNTs)^{16,17}, which exhibits a single ODMR line at $g=2$ (details in Material and Methods and Supplementary Note 3). Sweeping the magnetic field strength shows that the resonance structure of *DmCry* follows the signal of the BNNTs, proving that we are indeed observing an electronic spin resonance (Fig. 2a). Interestingly, we observe a strong dependence on the shape of the resonance structure. Although the underlying effects are not yet understood, we attribute them to the complex spin environment which includes multiple hyperfine interaction of the RP¹⁵ (see Supplementary Note 3). Importantly, these results demonstrate that *DmCry* can be used as a genetically encoded, optically readable magnetometer.

The ODMR effect can be tentatively explained by the magnetic field sensitive singlet-to-triplet interconversion rate of the FAD-Trp RP (Fig. 1b). In the MFE experiments, the magnetic field splits the triplet states, which affects the spin selective recombination rates and consequently the fluorescence intensity. The applied RF fields induce transitions between the T^0 and T^+ and T^- triplet states and reverse the effect of the magnetic field and leads to an increase in fluorescence intensity. Importantly, our results demonstrate the *DmCry* radical pair spin states and their reaction products can be controlled using RF fields at room temperature — a key distinction from solid-state spin defects, where chemical reactivity remains unaffected (Fig. 1a).

In the next step, we examined a previously characterized *DmCry* mutant (W394F) that exhibits a reduced distance between the RP partners and a shorter lifetime of downstream radical products in the reaction cascade¹². Experiments reveal a weaker amplitude and faster

dynamics of the MFE effect of the W394F mutant (Fig. 2b). Similarly, the ODMR signal of the mutant is strongly reduced compared to the wild type under the same conditions (Fig. 2c). We conclude that the mutation affects the RP and propose that the reduced lifetime of the downstream radical pairs—resulting in a lower recombination rate—leads to a decrease in ODMR contrast. The results support that the ODMR signal originates from the RP in the protein and, crucially, that it can be modulated by the protein structure. However, we expect that ODMR is not unique to *DmCry*, but common to RP forming systems (Supplementary Note 1).

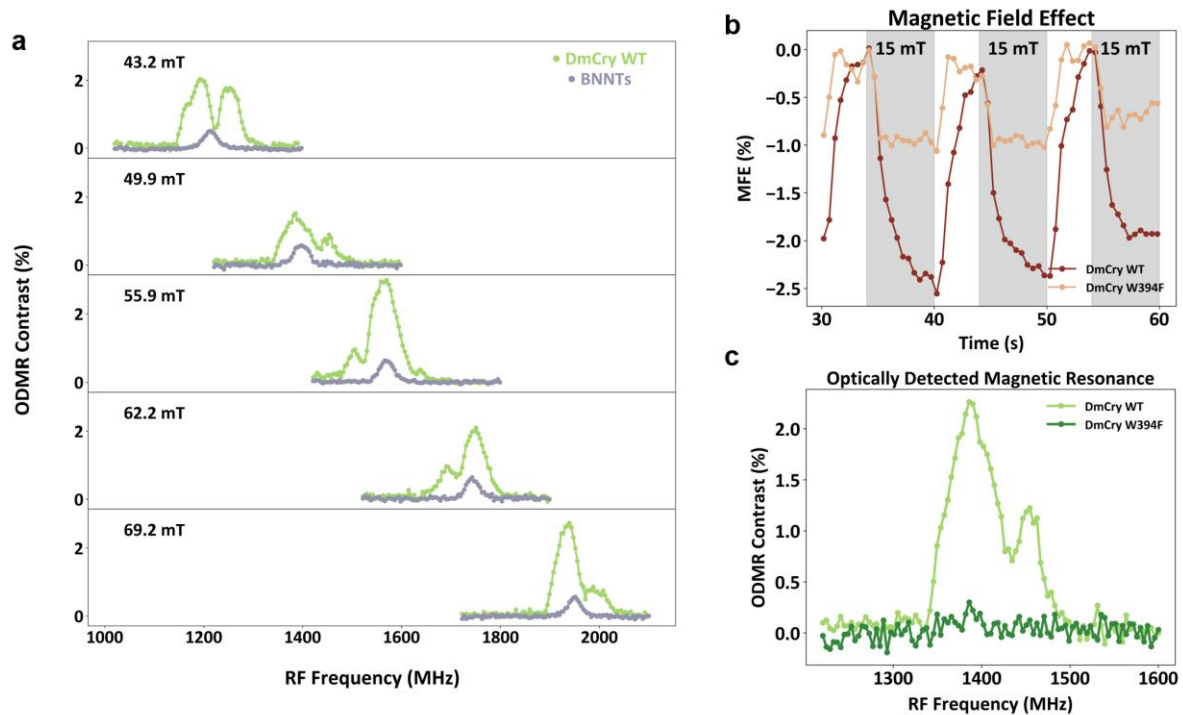


Figure 2. Optically detected spin resonance of *DmCry*. **a)** Magnetic field dependency of the optically detected spin resonance spectrum of *DmCry*. As reference a $g=2$ solid state spin defect in boron nitride nanotubes is shown (grey). **b)** MFE comparison of the *DmCry* wildtype and mutant (W394F). **c)** ODMR comparison of the *DmCry* wildtype and mutant under identical conditions (49.9 mT).

The potential applications of a detectable spin-photon interface in proteins extend well beyond quantum sensing and genetically encoded magnetometry in biological systems. ODMR signals offer an additional layer of information compared to conventional fluorescence techniques. For example, the ability to actively modulate fluorescence intensity using magnetic or RF fields enables highly sensitive lock-in detection¹⁸, which can significantly enhance measurement sensitivity. Moreover, RF resonances detectable by fluorescence can provide an efficient means of encoding information, offering a robust and versatile approach to multiplexing fluorescence microscopy¹⁹. Traditional fluorescence microscopy is constrained by the spectral characteristic of fluorophores; however, ODMR signals with distinct spectral features may allow multiplexing at a single optical wavelength, overcoming this limitation.

Finally, our work demonstrates that spin states and reaction yields can be actively manipulated using RF fields, even under ambient conditions. This paves the way towards RF-based control of biological processes such as gene expression or signalling^{20–22}.

Note: While finalizing our manuscript, we became aware of related preprints reporting on magnetic resonance controlled chemical yields in red fluorescent protein-flavin systems²³ and on ODMR in alternative protein systems^{24,25}.

Methods

Sample preparation. All *DmCry* variants were produced according to Paulus et al.²⁶ and Nohr et al.²⁷. Protein samples were stored in a buffer containing 50 mM HEPES, 100 mM NaCl, 50% (v/v) glycerol at pH 7.0 at -80 °C. Prior to experiments, protein solutions were thawed and centrifugated to remove denatured protein aggregates. After centrifugation, 20 μ L of the supernatant was transferred to a quartz cuvette (Z805963, Hellma Analytics) and sealed with a 12 mm round cover glass (W07-4615002, Labstellar). The experiments were performed using 120 μ M *DmCry* WT. For ODMR comparison between *DmCry* WT and W394F variants, the WT protein concentration was diluted from 120 μ M to 68 μ M to match the concentration of the W394F mutant.

Optical setup. A 447 nm blue laser (iBEAM-SMART-445-S_14935, TOPTICA Photonics AG) was directed through a dichroic mirror (MD498, Thorlabs) and focused onto the sample using a 50x objective (MXPLFLN, Olympus). A 180 mm tube lens (TTL180-A, Thorlabs) was paired with the objective to achieve optimal magnification. The laser power was set to 50 μ W, with a laser spot size of approximately 13 μ m \times 13 μ m. Upon excitation, green fluorescence emitted from the samples was collected by the same objective, passed through the dichroic mirror and a 525 nm bandpass filter (MF525-39, Thorlabs), and imaged using a sCMOS camera (Kinetix, Teledyne Photometrics).

Magnetic field effect experiments. The quartz cuvette was positioned on an aluminum cage plate. To prevent protein thermal degradation, temperature control was implemented using a single-stage Peltier element (TECF2S, Thorlabs) positioned beneath the aluminum cage plate, maintaining the sample at 15 °C. A custom-built cooper coil provided a modulated magnetic field (0 - 15 mT) at the sample position. Under continuous 447 nm laser illumination, fluorescence intensity was recorded using the camera with 500 ms exposure time. The initial decay in fluorescence intensity in the raw data was primarily attributed to photobleaching and photoreduction effects. A custom Python script was used to synchronize the magnetic field modulation with image acquisition.

RF strip line antenna design. RF strip line structure was designed in-house and fabricated (CERcuits, Geel) to provide RF fields for coherent electron spin manipulation. The strip line structure is implemented on a PCB with outer dimensions of 50.6 mm \times 40.6 mm. Aluminum oxide was chosen as substrate material with a thickness of 500 μ m, due to its high thermal conductivity. The conductive layer and ground plane are both composed of copper, each with a thickness of 70 μ m. The signal conductor was implemented as a straight line with a width of 480 μ m, resulting in a characteristic impedance of ~ 50 Ω . A ~ 2 mm-long constriction was introduced at the center of the line to reduce the width to 240 μ m, thus enhance the local RF field strength in the sample region. This narrowed region is designed to boost current density locally, which in turn increases RF magnetic field in the vicinity of the sample positioned above

it. The microstrip layout was optimized to maintain impedance matching and minimize signal reflection, while also providing sufficient field strength for fast, coherent spin-state manipulation.

Optically detected magnetic resonance experiments. The experimental setup employed a Pulse Streamer 8/2 (Swabian Instruments) for precise synchronization of the laser illumination, RF, and camera imaging acquisition. A custom lab software (QuPyt, <https://github.com/KarDB/QuPyt>) was used for precise timing. Radio wave frequencies were generated using a signal generator (R&S@SMB100A, Rohde & Schwarz) set to an output power of -5 dBm. The pulses were generated by a RF switch (ZASWA-2-50DRA+, Mini-Circuits), amplified with a broadband RF amplifier (KU PA BB 070270-80 B, Kuhne electronic), and delivered to the sample via a RF strip line antenna. The antenna was terminated with a 50 Ω high-power load (TERM-50W-183S+, 50 W, SMA-M, Mini-Circuits) to prevent reflections. The sample in the cuvette was placed on the RF strip line. The strip line was placed on the aluminum cage plate and the temperature of sample was kept at 15 °C. This configuration provided both effective heat dissipation and stable RF delivery.

The measurement protocol employed a synchronized cycle consisting of: a 1-second RF pulse with simultaneous laser illumination and camera exposure, followed by a 9-second recovery period and a reference measurement with laser illumination and camera exposure without RF. A tunable permanent magnet system generated static magnetic fields ranging from ~ 43.2 to 69.2 mT. At each magnetic field strength, we performed RF frequency sweeps across a 400 MHz range while monitoring the fluorescence intensity change.

Setup calibration using boron nitride nanotubes. Reference experiments were conducted using boron nitride nanotubes (BNNTs) purchased from NanoIntegris Inc.. The BNNTs have an average diameter of ~50 nm and lengths of a few micrometers. As-received BNNT powder was dispersed in 0.25% Triton X-100, stirred on a plate for 4 hours, followed by 10 minutes sonication. Afterwards, the BNNT solution was applied to a glass coverslip in a laminar flow hood, allowing solution to evaporate and fixing BNNTs on the coverslip. Then the coverslip with BNNTs was then placed on the strip line. The BNNTs were characterized before^{16,17}. The laser power was adjusted to 500 μ W to excite the BNNTs and fluorescence was collected using a 647 nm long pass filter (647 LP Edge Basic Longpass Filter, Semrock).

Control experiments. Control experiments for ODMR measurements were performed using an FAD and Trp mixture, which forms spin-correlated radical pairs upon photoexcitation. These control experiments included: FAD and Trp mixture in aqueous solution, FAD and Trp in 50% (v/v) glycerol. In both cases, FAD and Trp were prepared at a concentration of 120 μ M, identical to the *DmCry* WT sample (see Supplementary Note 1).

UV-Vis spectroscopy. Absorption spectra were recorded from 300 to 800 nm using a UV-Vis spectrophotometer (UV-1800, Shimadzu). To rule out whether free FAD released from denatured proteins caused the observed effects, we recorded absorption spectra from freshly prepared protein samples using the preparation procedure described above (details in Supplementary Note 1). The cuvettes were sealed using the same quartz coverslip material as the cuvette itself.

Data analysis. The ODMR contrast was calculated by first dividing the fluorescence intensity measured with RF on by the fluorescence intensity with RF off. This ratio was then corrected by subtracting the baseline. The MFE was corrected by subtracting the photobleaching decay, which was fitted with a linear curve over the selected time range.

Acknowledgements

Funding. This project has been funded by the Bayerisches Staatministerium für Wissenschaft und Kunst through project IQSense via the Munich Quantum Valley (MQV) and the European Research Council (ERC) under the European Union's Horizon 2020 research and innovation programme (Grant Agreement No. 948049). The authors acknowledge support by the DFG under Germany's Excellence Strategy–EXC 2089/1-390776260 and the EXC-2111 390814868.

Author Contributions. D.B.B. conceived the study. K. M. designed and built the setup and performed the experiments. L.N. took care of the sample handling. J.B. provided the sample. N.R.v.G. designed the RF antenna. K.M., R. R., C. E., L.N., E.S. and D.B.B. analyzed and discussed the data. R. R. helped setting up the experiment and implemented the BNNT experiments. E.S. and D.B.B. supervised the study. D.B.B. wrote the manuscript with input from all authors.

References

1. Schirhagl, R., Chang, K., Loretz, M. & Degen, C. L. Nitrogen-Vacancy Centers in Diamond: Nanoscale Sensors for Physics and Biology. *Annu. Rev. Phys. Chem.* **65**, 83–105 (2014).
2. Vaidya, S., Gao, X., Dikshit, S., Aharonovich, I. & Li, T. Quantum sensing and imaging with spin defects in hexagonal boron nitride. *Advances in Physics: X* **8**, 2206049 (2023).
3. Degen, C. L., Reinhard, F. & Cappellaro, P. Quantum sensing. *Rev. Mod. Phys.* **89**, 035002 (2017).
4. Mani, T. Molecular qubits based on photogenerated spin-correlated radical pairs for quantum sensing. *Chemical Physics Reviews* **3**, 021301 (2022).
5. Bayliss, S. L. *et al.* Optically addressable molecular spins for quantum information processing. *Science* **370**, 1309–1312 (2020).
6. Khakzad, H. *et al.* A new age in protein design empowered by deep learning. *Cell Systems* **14**, 925–939 (2023).
7. Packer, M. S. & Liu, D. R. Methods for the directed evolution of proteins. *Nat Rev Genet* **16**, 379–394 (2015).
8. Hore, P. J. & Mouritsen, H. The Radical-Pair Mechanism of Magnetoreception. *Annual Review of Biophysics* **45**, 299–344 (2016).
9. Henbest, K. B. *et al.* Magnetic-field effect on the photoactivation reaction of Escherichia coli DNA photolyase. *Proceedings of the National Academy of Sciences* **105**, 14395–14399 (2008).
10. Kattinig, D. R. *et al.* Chemical amplification of magnetic field effects relevant to avian magnetoreception. *Nature Chem* **8**, 384–391 (2016).
11. Xu, J. *et al.* Magnetic sensitivity of cryptochrome 4 from a migratory songbird. *Nature* **594**, 535–540 (2021).
12. Nohr, D. *et al.* Extended Electron-Transfer in Animal Cryptochromes Mediated by a Tetrad of Aromatic Amino Acids. *Biophysical Journal* **111**, 301–311 (2016).
13. Déjean, V. *et al.* Detection of magnetic field effects by confocal microscopy. *Chem. Sci.* **11**, 7772–7781 (2020).
14. Bucher, D. B. *et al.* Quantum diamond spectrometer for nanoscale NMR and ESR spectroscopy. *Nat Protoc* **14**, 2707–2747 (2019).

15. Wong, S. Y., Benjamin, P. & Hore, P. J. Magnetic field effects on radical pair reactions: estimation of B1/2 for flavin-tryptophan radical pairs in cryptochromes. *Phys. Chem. Chem. Phys.* **25**, 975–982 (2023).
16. Gao, X. *et al.* Nanotube spin defects for omnidirectional magnetic field sensing. *Nature Communications* **15**, 7697 (2024).
17. Rizzato *et al.* in preparation.
18. Miller, B. S. *et al.* Spin-enhanced nanodiamond biosensing for ultrasensitive diagnostics. *Nature* **587**, 588–593 (2020).
19. McGuinness, L. P. *et al.* Quantum measurement and orientation tracking of fluorescent nanodiamonds inside living cells. *Nature Nanotech* **6**, 358–363 (2011).
20. Engels, S. *et al.* Anthropogenic electromagnetic noise disrupts magnetic compass orientation in a migratory bird. *Nature* **509**, 353–356 (2014).
21. Ritz, T., Thalau, P., Phillips, J. B., Wiltschko, R. & Wiltschko, W. Resonance effects indicate a radical-pair mechanism for avian magnetic compass. *Nature* **429**, 177–180 (2004).
22. Zwang, T. J., Tse, E. C. M., Zhong, D. & Barton, J. K. A Compass at Weak Magnetic Fields Using Thymine Dimer Repair. *ACS Cent. Sci.* **4**, 405–412 (2018).
23. Burd, S. C. *et al.* Magnetic resonance control of reaction yields through genetically-encoded protein:flavin spin-correlated radicals in a live animal. 2025.02.27.640669 Preprint at <https://doi.org/10.1101/2025.02.27.640669> (2025).
24. Feder, J. S. *et al.* A fluorescent-protein spin qubit. Preprint at <https://doi.org/10.48550/arXiv.2411.16835> (2025).
25. Abrahams, G. *et al.* Quantum Correlations in Engineered Magneto-Sensitive Fluorescent Proteins Enables Multi-Modal Sensing in Living Cells. 2024.11.25.625143 Preprint at <https://doi.org/10.1101/2024.11.25.625143> (2024).
26. Paulus, B. *et al.* Spectroscopic characterization of radicals and radical pairs in fruit fly cryptochrome – protonated and nonprotonated flavin radical-states. *The FEBS Journal* **282**, 3175–3189 (2015).
27. Nohr, D. *et al.* Determination of Radical–Radical Distances in Light-Active Proteins and Their Implication for Biological Magnetoreception. *Angewandte Chemie International Edition* **56**, 8550–8554 (2017).